Inductively Powered Arbitrary-Waveform Adaptive-Supply Electro-Optical Neurostimulator

Hossein Kassiri[1], M. Tariqus Salam[2], Fu Der Chen[1], Behraz Vatankhahghadim[1], Nima Soltani[1], Michael Chang[2], Peter Carlen[2], Taufik A. Valiante[2], Roman Genov[1]

[1] Department of Electrical & Computer Engineering, University of Toronto, Canada,

[2] Toronto Western Research Institute and the Department of Physiology, University of Toronto, Toronto, ON, Canada

***Abstract*—A hybrid current-mode and optogenetic miniature neurostimulating system is presented. The 16-channel electrical stimulator outputs arbitrary-waveform charge-balanced current-mode stimulation pulses with the amplitude ranging from 0.05mA to 10mA. To optimize power consumption, the supply voltage is automatically adjusted through an impedance monitoring feedback loop that gauges the minimum required headroom voltage. The 8-channel optogenetic stimulator reuses the arbitrary-waveform generation functions of the electrical stimulator. Each pulse-generator drives one LED with a maximum of 25mA. The LEDs are assembled within a custom-made 4×4 ECoG grid electrode array, which enables precise optical stimulation of neurons with a 300μm spatial resolution and simultaneous monitoring of the neural response by the ECoG electrode, at different distances of the stimulation site. The implantable system is a 3×2.5×1 cm^3 stack of a receiver coil and two mini-boards. The power is received by a 32-layer flexible inductive coil and is regulated by the wireless communication board. The adaptive neurostimulator board boosts the regulated voltage up to the level set by the feedback loop with a maximum of 24V. The system also receives stimulation parameters wirelessly from the amplitude-shift-keyed power carrier. Both electrical and optogenetic stimulation results from chronic and acute in vivo rodent experiments are presented.**

I. Introduction

Electrical stimulation is an established effective drugs-alternative treatment option for a variety of neurological disorders. The exact mechanism behind electrical neuro-stimulation in many cases remains unknown in part due to the lack of a proper tool enabling cell-type-selective neural excitation or inhibition in addition to simultaneous high-resolution spatiotemporal neural recording. The relatively new optogenetic neurostimulation technique has opened a new avenue for better understanding of mechanisms of neural function [1]. Additionally, optogenetic cell-type-specific modulation of neuronal activity opens up the prospect of preventing abnormal brain states that result in certain neurological conditions [2]. Unlike electrical stimulation, optogenetic stimulation selectively modulates neuronal activity in a local neural network and this modulation does not generate artifacts in the recording. Thus, a combination of electrical and optical stimulation such as the system presented here as shown in Fig.1, may be a potent novel technique for better understanding of the brain function and dysfunction, and for generating optimal brain modulation for treating neurological disorders.

Voltage-controlled stimulation (VCS) [3], current-controlled stimulation (CCS) [4] and switched-capacitor charge-base stimulation (SCS) [5] are the three existing methods to provide electrical stimulation to the body. VCS can not control the amount of the injected charge during stimulation and could cause sub-optimal results and tissue damage. SCS has the disadvantage of limited control over the stimulation pulse shape. Current-based stimulators, on the other hand, have excellent control of charge injected into the tissue and can deliver a precisely-programmed current pulse shape.

Current-controlled stimulators typically suffer from poor power efficiency compared to VCS and SCS. This is because the supply voltage of these stimulators is set to accommodate a sufficient headroom voltage for the worst-case scenario, which is stimulating with the highest-amplitude current into the largest possible tissue impedance. Having such high supply voltage when stimulating with lower-than-maximum current amplitudes or into smaller-than-maximum tissue impedances, results in a significant portion of the consumed power being wasted. Some power-adaptive designs have been reported that

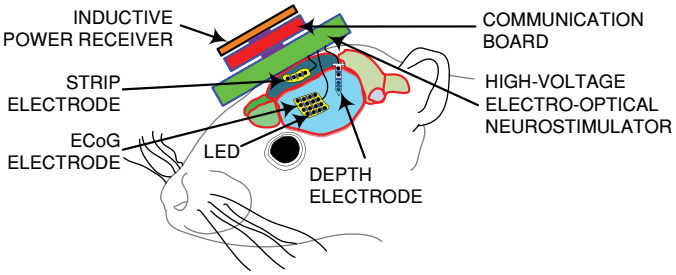

Fig. 1: Envisioned implantation configuration of the wireless electro-optical neurostimulator and its three main components.

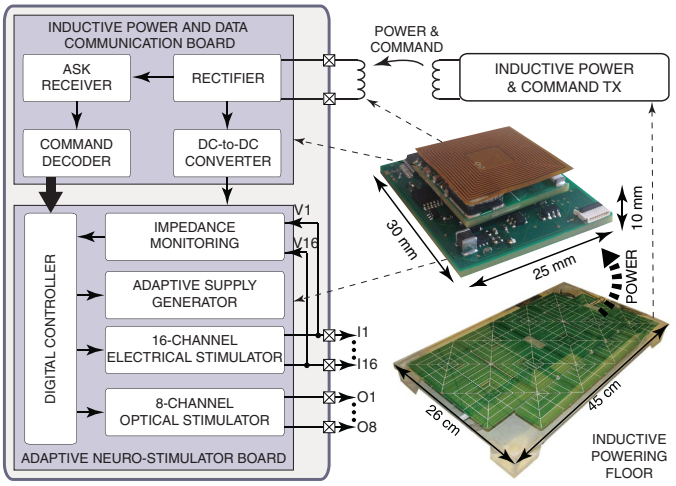

Fig. 2: Simplified block diagram and physical view of the inductively-powered electro-optical stimulating system.

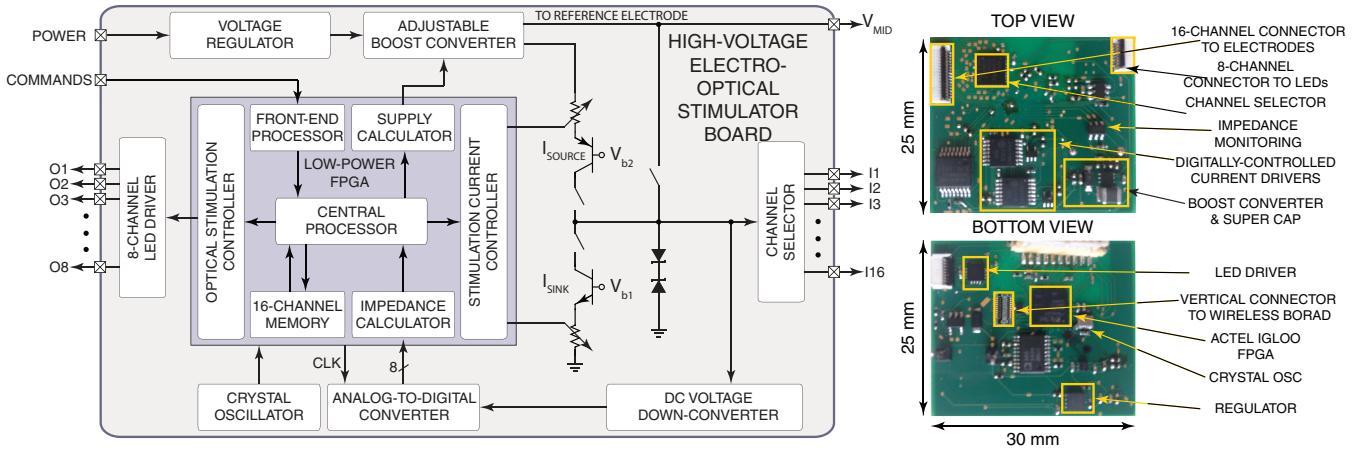

Fig. 3: Simplified block diagram of the power-adaptive high-voltage electro-optical stimulator board.

vary the supply voltage to the minimum required value based on the output of a sensory feedback loop [5], [6]. However, the feedback implementation in these designs either results in a reduced available stimulation headroom voltage, or increases power consumption significantly [6].

In this paper we present a combined 16-channel current-mode and an 8-channel optogenetic stimulating system for neural stimulation. Both stimulators can generate arbitrary waveforms (10-bit resolution) for stimulation. A digital controller adjusts the system's supply voltage to the minimum required value based on the output of a low-power ADC-based impedance monitoring feedback loop with no headroom voltage overhead. Additional circuits are added to the system to ensure safe and charge-balanced stimulation. For freely moving rodent studies, the neurostimulator system is powered by an inductive powering system and receives configuration commands wirelessly using the same inductive link.

II. System Architecture

Fig. 2 shows a simplified block diagram of the adaptive-supply electro-optical neurostimulation system. As shown, the system has 16 electrical and 8 optical stimulation channels. All channels generate independently-programmed arbitrary waveforms for hybrid neurostimulation. The system connects with both ECoG electrodes and LED-arrays that are implanted over the brain cortex surface. To minimize the power consumption, tissue impedance variations seen at each electrode are continuously monitored and fed to a digital controller that adjusts the supply voltage as well as the DC level of the reference electrode. Fig. 2 also depicts how the stimulator board is connected to a wireless power and command receiver board through a vertical connector. The wireless board rectifies and regulates inductively-transmitted power that is sent by a cellular inductive powering rodent cage floor [9], and received by the receiver coil mounted on an animal. The inductive link provides up to 30mW of power at the maximum distance of 15cm. The system utilizes the same inductive link to receive configuration commands.

III. Design Implementation

Fig. 3 shows a simplified block diagram of the neuro-stimulator board. The figure also shows the top and bottom views of the board with all the main components labeled. A low-power FPGA is used to control the system mode of operation, channel seletion, as well as each channel's individual stimulation amplitude, frequency, waveform, and supply voltage.

Using an adjustable boost converter, the neurostimulator can increase the DC voltage that it receives from the wireless board from 3.3V to up to 24V. Such high supply voltage provides a large voltage headroom for current drivers and consequently enables higher stimulation currents. Considering 1.5-2V drop on current sources (I_{source} and I_{sink}), for a typical 1kΩ tissue resistance, the system can provide up to 10mA current. As previously mentioned, to save power, lower stimulation currents should be delivered at smaller supply voltages, and if the supply is kept at the maximum value of 24V, it results in a significant unnecessary power dissipation. Besides the stimulation current, variations in tissue impedance, a common in vivo phenomenon, also affect the required supply voltage. For a fixed stimulation current, tissue impedance variations change the voltage drop across it and consequently affect the required headroom voltage.

Unlike the stimulation current that is known (e.g., set by a clinician), the tissue impedance must be continuously monitored. An 8-bit ADC is used to sample the DC voltage across the electrode and feed the results to the FPGA. The FPGA determines the minimum supply voltage required for the current drivers and adjusts the boost converter output accordingly. Once the stimulation for the channel is completed, FPGA will save the last voltage level into the channel profile so that the minimum voltage can be provided at the start of next iteration.

The results in [7], [8] show that the pulse shape does affect the stimulation effectiveness. With the optimal waveform, the current amplitude needed can be reduced and ultimately this leads to additional power savings. For the current-mode stimulation, common-base BJT current drivers are controlled using digitally-adjustable potentiometers connected in series

with the emitter to generate a current from 50μA to 10 mA. The 10-bit potentiometer itself is controlled digitally by the FPGA and has 1024 positions. To control duty-cycle of the stimulation waveform, a timer is implemented on the FPGA to keep track of the stimulation duration.

To avoid charge accumulation, the current-mode stimulator is always programmed for equal overall charges flowing in and out of the tissue. However, the mismatch between the anodic and cathodic currents could result in a residual charge that must be removed. As shown in Fig. 3, a discharging path to the reference electrode V_{MID} for the targeted tissue is employed to compensate for the mismatched error. The same switch is used to discharge accumulated charge on the ac-coupling capacitor due to switches leakage current.

A sudden high current inrushes into the tissue when switching the stimulation path on and off can alter the stimulation effect or damage the tissue. A voltage limiter built using Zener diodes is employed in the system to prevent a high current flowing into the tissue. When high current is flowing into the electrode, it will induce a high voltage. Once the voltage across electrode reaches above 27V, the Zener diode will fall into the breakdown region, diverting the high current into the ground.

For the optical stimulation, an LED light source is driven by a current as governed by its exponential I-V relationship. Increasing stimulation current does not change the required supply voltage significantly and a 3.3V supply is sufficient for the operation. As a result, independent electrical and optical stimulation not only enables simultaneous modes of operation, but also saves a significant amount of energy that would be wasted in LEDs otherwise. An 8-channel digitally-controllable LED driver is utilized to provide up to 25mA current to the LED array and is supplied with a fixed 3.3V voltage.

For an implantable/wearable system for rodent studies, power and configuration commands should ideally be provided wirelessly to avoid bulky and heavy batteries and wires. The inductive link provides up to 30mW with the maximum distance of 15cm away from the transmitter. The power carrier is amplitude shift-keyed to communicate the configuration commands from a computer to the implantable system using the same wireless link. A 470mF super capacitor is utilized that gets charged during the idle phase and provides stable supply voltage during stimulation phase for a maximum of 2 minutes continuous pulse-train with the maximum signal's amplitude. A comparator is utilized to monitor the power usage of the system. If the voltage of the super capacitor falls below 3.6V, the FPGA will stop the stimulation to avoid abnormal behavior under low power conditions.

The electro-optical electrode array was fabricated on a Polyimide sheet of 100μm thickness. A gold metalization layer was formed (800 nm) using DC sputtering deposition and was patterned using photolithography and wet etching to create the routing tracks (Fig. 4(a)). Light emitting diodes (LED) were soldered onto the gold contacts and sandwiched in between two ECoG layers using epoxy. The LEDs assembled within a two-layer ECoG electrode array (opcog) are shown in Figs. 4(b) and (c).

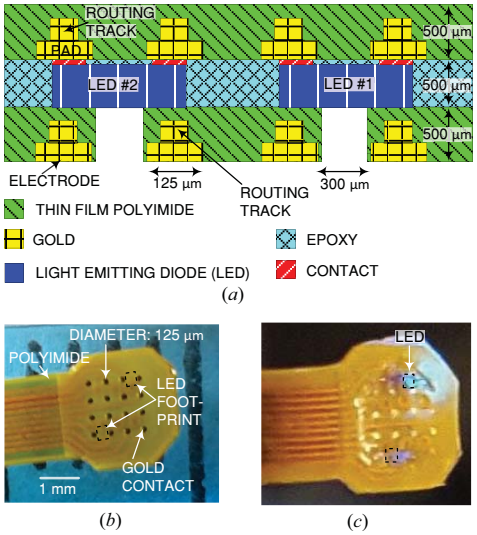

Fig. 4: ECoG grid: (a) Layers of ECoG (not to scale), (b) fabricated ECoG electrode array, and (c) LEDs assembled within the dual-layer ECoG electrode array (opcog) and blue light passing through the opcog from LED 1.

IV. Experimental Results

A. Electrical Stimulation Result

Fig. 5 shows an example of four experimentally-measured simultaneously-generated electrical stimulation waveforms. As illustrated, each channel is independently programmable with a 50μA resolution and the 10mA maximum amplitude. The highest resolution of the pulse width which the system can invoke is 100μs. This limitation is imposed by the data transmission and the programming time of the potentiometers.

Fig. 6 shows the adaptive power supply value when the load impedance is changed in small steps from 100Ω to 5kΩ and then back to 100Ω. As shown, the supply voltage increases with a maximum delay of 1ms/volts. The mid-range voltage V_{MID} used for the reference electrode also follows the supply voltage variations with a less than 1 ms delay. Fig. 7 shows how the stimulation current driver output varies when the digitally-controllable potentiometer in series with a common-base BJT emitter varies from 20kΩ to 60Ω.

B. In Vivo Experimental Results

Two in vivo experiments were performed to validate the stimulator. The procedures for both experiments were approved by the ethics committee of the Hospital for Sick Children and Toronto Western Research Institute, and the experiments were conducted at the Neuroscience and Mental Health Research Institute and Toronto Western Research Institute, respectively.

1) Electrical Stimulation: The electrical stimulator was validated by stimulating on a Wistar rat (250 gm) hippocampus in an in vivo chronic experiment. For this purpose, four bipolar microelectrodes were implanted into right the hippocampus, left cortex, right brainstem, and the skull as a reference. The hippocampus was stimulated and icEEG from the hippocampus, cortex and brainstem were recorded using a

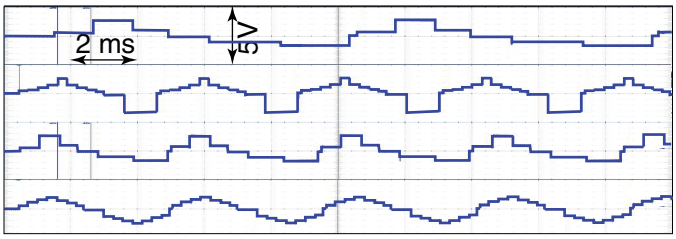

Fig. 5: Four experimentally-measured arbitrary waveforms generated simultaneously by the neurostimulator.

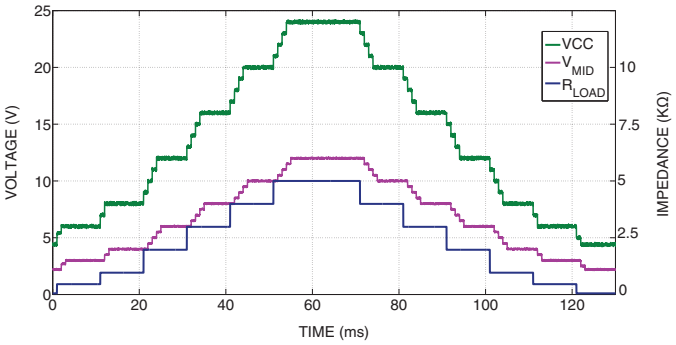

Fig. 6: Experimentally-measured voltage waveforms of the adaptive supply and reference voltage. The system keeps the supply voltage at the optimum value for a 2mA stimulation current while load impedance varies.

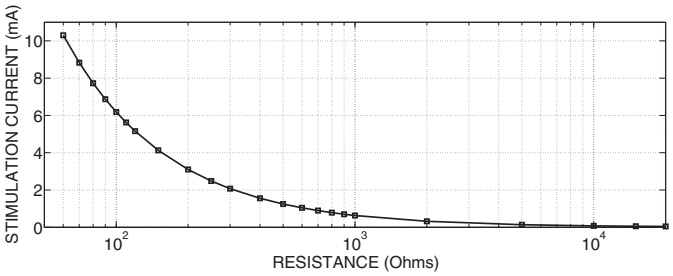

Fig. 7: Experimentally-measured stimulation current for different values of a digitally-controlled potentiometer.

commercial amplifier (Biopac Inc.). In the chronic experiment, the electrical stimulator triggered pulses with 150msec width and 200μA current at 5Hz for 5sec into the hippocampus. The stimulation effect propagated to the brainstem quickly, which partially inhibited cortical activity (shown in Fig. 8).

2) Optical Stimulation and Electrical Recording: In the second experiment, the optical stimulator was tested by shining blue light on the cortex of a transgenic mouse (p50) in an in vivo acute experiment. The mouse was anesthetized using Ketamine (95 mg/kg) and Xylazine (5 mg/kg) and mounted in a stereotactic frame. The scalp was removed and the opcog was placed through a 4 mm diameter craniotomy on the somatosensory cortex. The stimulator triggered a blue light pulse for 30ms and the icEEG using ECoG electrode array contacts were recorded using a neural amplifier. In the acute experiment, the blue light triggered neural spikes around the LED, and these spikes gradually propagated to distant regions within an approximately 1mm distance (shown in Fig.9).

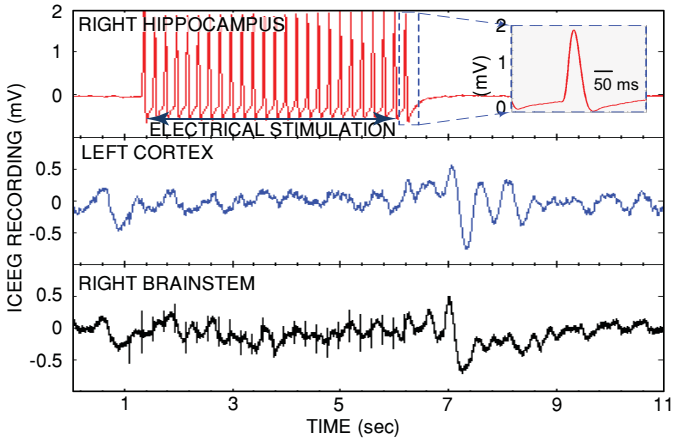

Fig. 8: Electrical stimulation of the hippocampus and icEEG recordings in the hippocampus, cortex and brainstem.

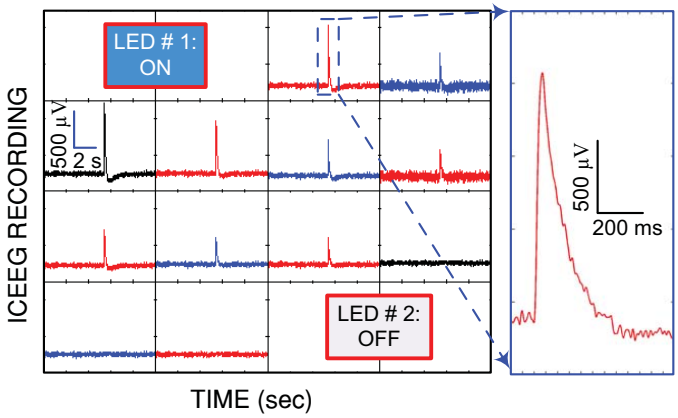

Fig. 9: A brief (30 ms) optical stimulation using LED1 and spatiotemporal propagation of neuronal excitation in a ChR2-expressing mouse.

References

[1] A. R. Adamantidis, et al. "Neural substrates of awakening probed with optogenetic control of hypocretin neurons," Nature Vol. 450, No. 7168 pp. 420–424, 2007.

[2] A. Witt, et al. "Controlling the oscillation phase through precisely timed closed-loop optogenetic stimulation: a computational study," Frontiers in neural circuits, Vol. 7, 2013.

[3] F. Shahrokhi et al., "The 128-channel fully differential digital integrated neural recording and stimulation interface," IEEE Trans. Biomed. Circuits Syst., vol. 4, no. 3, pp. 149–161, Jun. 2010.

[4] H. Kassiri et al., "Inductively-Powered Direct-Coupled 64-Channel Chopper-Stabilized Epilepsy-Responsive Neurostimulator with Digital Offset Cancellation and Tri-Band Radio," IEEE ESSCIRC, 2014, pp. 95–98.

[5] Lee, Hyung-Min, et al. "A Power-Efficient Switched-Capacitor Stimulating System for Electrical/Optical Deep Brain Stimulation," Solid-State Circuits, IEEE Journal of 50.1 (2015): 360–374.

[6] Chen W-M et al., "A fully integrated 8-channel closed-loop neural-prosthetic CMOS SoC for real-time epileptic seizure control," IEEE JSSC, vol. 49, no. 1, pp. 232–47, 2014.

[7] A. Wongsarnpigoon et al, "Efficiency analysis of waveform shape for electrical excitation of nerve fibers," IEEE Trans. Neural Syst. Rehab. Eng., vol. 18, no. 3, pp. 319–328, June 2010.

[8] A. Wongsarnpigoon and W. M. Grill, "Energy-efficient waveform shapes for neural stimulation revealed with a genetic algorithm," J. Neural Eng., vol. 7, no. 4, June 2010

[9] N. Soltani et. al., "Cellular Inductive Powering System for Weakly-Linked Resonant Rodent Implants," IEEE BioCAS, 2013.